

Time-Periodic Stiffness Modulation in Elastic Metamaterials for Selective Wave Filtering: Theory and Experiment

Giuseppe Trainiti,¹ Yiwei Xia,^{2,*} Jacopo Marconi,³ Gabriele Cazzulani,³ Alper Erturk,² and Massimo Ruzzene^{1,2}

¹*Daniel Guggenheim School of Aerospace Engineering Georgia Institute of Technology, Atlanta, Georgia 30332, USA*

²*George W. Woodruff School of Mechanical Engineering Georgia Institute of Technology, Atlanta, Georgia 30332, USA*

³*Department of Mechanical Engineering Politecnico di Milano, Milano 20156, Italy*



(Received 21 May 2018; published 26 March 2019)

Elastic waveguides with time-modulated stiffness feature a frequency-periodic dispersion spectrum, where branches merge at multiple integers of half the modulation frequency and over a finite wave number range. In this range, frequency becomes complex, with its real part remaining constant. The vanishing group velocity associated with these flat bands leads to frequency-selective reflection at an interface between a nonmodulated medium and a time-modulated one, which converts a broadband input into a narrow-band output centered at the half modulation frequency. This behavior is illustrated in an elastic waveguide in transverse motion, where modulation is implemented experimentally by an array of piezoelectric patches shunted through a negative electrical capacitance controlled by a switching circuit. The switching schedule defines the modulation frequency and allows the selection of the output frequency. This implementation is suitable for the investigation of numerous properties of time-space modulated elastic metamaterials, such as nonreciprocity and one-way propagation, and can lead to the implementation of novel functionalities for acoustic wave devices operating on piezoelectric substrates.

DOI: [10.1103/PhysRevLett.122.124301](https://doi.org/10.1103/PhysRevLett.122.124301)

Research on time-dependent material properties has received considerable attention over the years. Parametric effects in time-modulated media have long been used for amplification of electromagnetic waves [1,2] and surface acoustic waves [3,4]. Parametric amplification in electromagnetic waveguides has been investigated in periodic [5–10] and nonperiodic modulation schemes [11], while spatiotemporally modulated gratings have been proposed for radio-frequency communication systems that are shielded from echoes and reflections during transmission [12]. In acoustics, isolation levels as high as 40 dB within the audible range have been achieved with acoustic circulators consisting of cavities with time-dependent volumes [13], and asymmetric transmission has been reported in an acoustic waveguide with a time-dependent scattering element [14]. Recently, traveling-wave modulation of physical properties has been explored for nonreciprocal wave motion in optics, acoustics, mechanics, and heat transfer [15–22]. Nonreciprocal components connected in 1D and 2D lattice arrangements [23] have been investigated for nontrivial wave topologies that support defect and backscattering immune propagation [24,25]. In mechanics, numerous theoretical studies have investigated time-dependent material properties and their potential to produce nonreciprocity [26]. However, the physical implementation of dynamically changing stiffness or mass distributions mostly remains an open challenge. Among the suggested approaches, light induced softening in $\text{Ge}_x\text{Se}_{1-x}$ glasses has been explored [27], while Coriolis-

type effects have been exploited to produce a time-dependent moment of inertia in a pendulum with a radially moving mass [28]. More recently, a phononic crystal with spatiotemporal modulation of electrical boundary conditions in a stack of piezoelectric elements has been described in [29]. Magnetoelastic media interacting with an external magnetic field [30] and magnetorheological fluids [31] are also suggested solutions for traveling wave modulation [32].

In this Letter, we show that time-modulated stiffness in elastic waveguides produces a frequency-periodic dispersion spectrum, where branches merge at $r\omega_m/2$, where ω_m is the modulation frequency and r is an integer. Merging occurs over a finite wave number range, within which frequency is complex, with a constant real part. This produces a flat dispersion branch that leads to a standing, or nonpropagating, wave which is parametrically amplified [1,3,4]. Analytical predictions of the frequency-periodic spectrum with merging branches and of a wave number gap associated with the flat band are reported for a dispersive elastic waveguide in transverse motion. Also, we demonstrate, both numerically and experimentally, the frequency-selective reflection properties of an interface between a nonmodulated waveguide and a modulated one, which converts a broadband incident wave (input) into a narrow-band reflected wave (output), centered at $r\omega_m/2$. Experimental implementation of the concept consists in an aluminum beam partially covered by an array of piezoelectric patches shunted through negative capacitance (NC) circuits, which control the equivalent stiffness of the beam [33]. Periodic switching of the circuit

connection with the patches produces a square-wave modulation of the waveguide stiffness according to a selected modulation frequency. The proposed experimental platform lends itself to the exploration of space-time modulations as an effective means to achieve nonreciprocal wave motion [34]. In addition, the use of actively controlled shunted patches may be pursued for the study of parity-time (PT) symmetric photonic and phononic systems that feature alternating regions of gain and loss. Novel functionalities would result from the nontrivial, nonconservative wave interactions and phase transitions, and may open new prospects for an active control of elastic waves, sound, and light [35].

We consider the transverse motion of a beam with time-dependent material properties, which is governed by

$$D(t) \frac{\partial^4 w(x, t)}{\partial x^4} + \frac{\partial}{\partial t} \left(m(t) \frac{\partial w(x, t)}{\partial t} \right) = 0, \quad (1)$$

where $D = EI$ is the bending stiffness, with E denoting Young's modulus, and I is the second moment of area of the beam cross section. Also, $m = \rho A$ denotes the beam linear mass, where ρ is the density and A is the cross-sectional area. We assume a constant mass $m(t) = m$, and introduce a time-dependent stiffness $D(t) = D(t + T_m)$, where $T_m = 2\pi/\omega_m$. A solution of the resulting equation of motion is sought in the form:

$$w(x, t) = e^{i(\omega t - \kappa x)} \sum_{n=-\infty}^{+\infty} \hat{w}_n e^{in\omega_m t}. \quad (2)$$

For simplicity, we assume harmonic modulation, i.e., $D(t) = D_0[1 + \alpha_m \cos(\omega_m t)]$, where $\alpha_m = D_m/D_0$ defines the modulation amplitude. Dispersion relations are obtained by solving a quadratic eigenvalue problem in terms of ω upon imposing a wave number κ . The resulting dispersion diagrams for $\alpha_m \rightarrow 0$ and $\alpha_m \neq 0$ in Fig. 1 show the real and the negative of the imaginary part of the frequency associated with each wave number. Notably, time modulation produces a family of branches that are ω_m periodic in the frequency domain. This is consistent with the theoretical findings on dielectric time modulation in electromagnetic waveguides [36]. The branches intersect at frequency $r\omega_m/2$, as illustrated for $\alpha_m \rightarrow 0$ in Fig. 1(a). For finite α_m , intersecting branches merge over a finite wave number range [Fig. 1(b)], within which frequency has a nonzero imaginary component and a constant real part. This range of wave numbers was denoted as a κ band gap in Ref. [36]. In analogy with frequency band gaps, plane wave harmonic excitation at frequency–wave-number pairs corresponding to the flat bands leads to a stationary, or nonpropagating, wave. In the absence of dissipation, the insurgence of an imaginary frequency component causes the amplitude of the wave to increase exponentially as a result of parametric amplification [3].

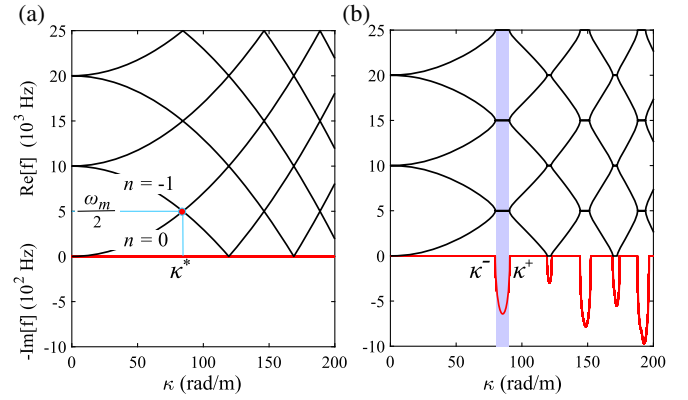


FIG. 1. Frequency-periodic dispersion diagrams for a time-modulated waveguide (beam in bending). Black and red lines respectively denote the real part and (the negative of) the imaginary part of frequency. (a) $\alpha_m \rightarrow 0$: the intersection between the $n = 0$ and $n = -1$ occurs at frequency $\omega_m/2$ and κ^* ; the imaginary component is nil as a result of the vanishing modulation amplitude. (b) $\alpha_m = 0.4$: merging of the dispersion branches at $r\omega_m/2$ and corresponding nonzero imaginary frequency. The κ -band-gap range $\kappa \in [\kappa^-, \kappa^+]$ predicted by Eq. (5) is highlighted by the shaded blue region.

We estimate the width of the κ band gap by restricting our attention to the branches associated with $n = 0$ and $n = -1$ orders in Eq. (2), which gives the following characteristic equation:

$$(\omega^2 - \gamma\kappa^4)[(\omega - \omega_m)^2 - \gamma\kappa^4] - \left(\frac{\alpha_m\gamma\kappa^4}{2}\right)^2 = 0, \quad (3)$$

with $\gamma = D/m$. For $\alpha_m \rightarrow 0$, these branches intersect at point $\kappa^* = \sqrt{\omega_m/(2\gamma^{1/2})}$ and $\omega^* = \omega_m/2$ [Fig. 1(a)], while for $\alpha_m \neq 0$, the solution of Eq. (3) is

$$\omega = \frac{1}{2} \left[\omega_m - \sqrt{\omega_m^2 + 4\gamma\kappa^4 - 2\sqrt{\gamma\kappa^4(4\omega_m^2 + \alpha_m^2\gamma\kappa^4)}} \right], \quad (4)$$

where ω is complex if $\omega_m^2 + 4\gamma\kappa^4 - 2\sqrt{\gamma\kappa^4(4\omega_m^2 + \alpha_m^2\gamma\kappa^4)} < 0$. This identifies the wave number range $\kappa \in [\kappa^-, \kappa^+]$, with

$$\kappa^\pm = \sqrt[4]{\frac{\omega_m^2}{2\gamma(2 \mp \alpha_m)}} \quad (5)$$

The corresponding complex frequency $\omega = \omega_r + i\omega_i$, has a real part $\omega_r = \omega_m/2$ that is constant with respect to the wave number.

We investigate the behavior of a wave incident on an interface between a waveguide with constant properties and one with modulated Young's modulus, which quantifies stiffness (Fig. 2). Based on the observations above and on published theoretical results for space-time modulated nondispersive waveguides [17], we expect the unique

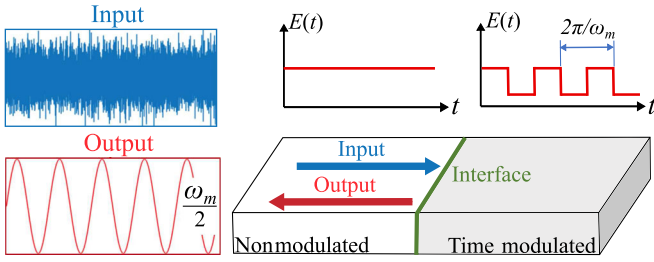


FIG. 2. Concept of a single-port system converting a broadband input into a narrow-band output through time-modulation. An incoming broadband wave is converted into a narrow-band output at a frequency defined by the modulation frequency $\omega_m = 2\pi/T_m$, which can be used as a tuning parameter for selecting the output frequency content.

characteristics of the time-modulated dispersion spectrum to be reflected in the reflection properties of the interface. Specifically, a plane wave propagating in the nonmodulated media at a frequency–wave-number pair corresponding to the κ band gap will be mostly reflected at the interface as a result of its inability to propagate in the time-modulated waveguide. The phenomenon could be also explained by power conversion between harmonic components, as done for waves propagating from homogeneous to time-modulated domains in nondispersive waveguides [17]. In this context, we consider the waveguide with interface as a conceptual single-port device that selectively filters a dominant frequency component out of a broadband input. The dominant output frequency of such a device (Fig. 2) is produced from the same broadband input by selecting the modulation frequency ω_m .

The concept is illustrated by evaluating the transient response of the waveguide with interface through a finite-difference time-domain (FDTD) approach. In the simulations, we consider a time-constant domain of length $L_h = 0.3$ m, while the modulated one is $L_m = 0.48$ m long. These dimensions are chosen in accordance with the considered experimental setup. The beam has a

rectangular cross section with $I/A = 8.67 \times 10^{-4}$ m. The density is $\rho = 2700$ kg/m³, while the Young’s modulus is $E_0 = 69.9$ GPa. In the time-modulated domain, the Young’s modulus obeys a square-wave modulation law:

$$E(t) = E_0 + \frac{\alpha_m E_0}{2} \{ \text{sgn}[\cos(\omega_m t)] - 1 \}, \quad (6)$$

with $\alpha_m = 0.14$, which is consistent with values produced during experiments. A wave is injected through a perturbation applied at the free end of the time-constant beam as a two-cycle tone burst with a center frequency of $f_{\text{exc}} = 5$ kHz. The frequency content of input $w_{\text{in}}(x_p, t)$ and output $w_{\text{out}}(x_p, t)$ are evaluated by probing a single location x_p close to the interface in the time-constant domain. The corresponding Fourier transform (FT) shown in Fig. 3(a) displays the frequency bandwidth of the input and of the output for modulation frequencies $f_m = 10, 12, 15$ kHz. The wave motion $w(x, t)$ in the time-constant waveguide can be represented in the frequency–wave-number domain $\hat{\mathcal{W}}(\kappa, \omega)$, which is obtained through spatial and temporal FT (2D-FT) [37]. The contour plots of the magnitude $|\hat{\mathcal{W}}(\kappa, \omega)|$ in Figs. 3(b)–3(d) effectively locate the spectral content of the wavefield along the theoretical dispersion branches. The $\kappa > 0$ region corresponds to forward (incident) waves, while the $\kappa < 0$ half plane is associated with backward (reflected) waves. This representation effectively illustrates how, at the interface, an incident broadband wave is converted into a reflected narrow-band wave centered at $f_m/2$. For reference, the half-power bandwidth of input and output is approximately 3.4 and 0.8 kHz, respectively, which corresponds to a output-to-input bandwidth ratio of approximately 24% for all considered modulation frequencies. Notably, the output center frequency is always at $f_m/2$, which illustrates the twofold effect of the time modulation on the reflected wave: a frequency conversion and a bandwidth reduction.

Time-periodic stiffness modulation of the elastic waveguide is implemented by employing an array of

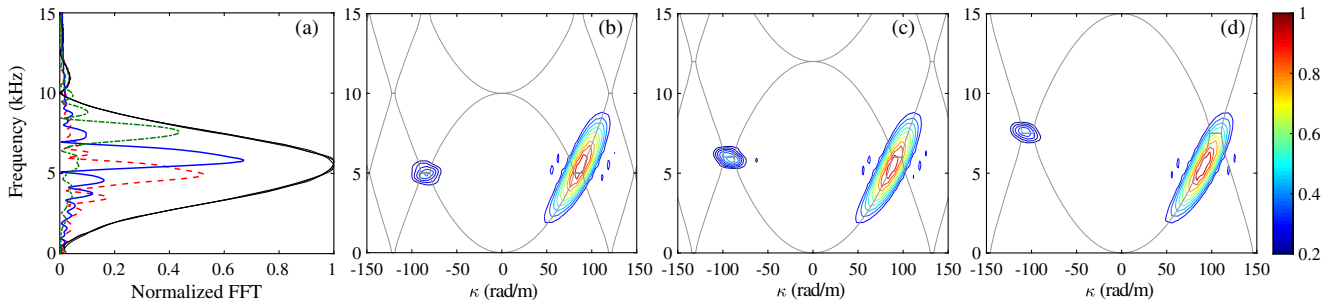


FIG. 3. Numerical results for the response of the single-port system for three modulation frequencies ($f_m = 10, 12, 15$ kHz). (a) Single point FTs show that a broadband input (black solid line) is converted into narrow-band outputs centered at $f_m/2$: $f_m = 10$ kHz (red dashed line), $f_m = 12$ kHz (blue solid line), and $f_m = 15$ kHz (green dash-dotted line). (b)–(d) Normalized 2D-FT magnitude $|\hat{\mathcal{W}}(\kappa, \omega)|$ associated with the wave field $w(x, t)$ shows narrow-band frequency reflection of the reflected waves in the $\kappa < 0$ half plane at $f_m/2$, which is in agreement with the location of the flat branches predicted theoretically (gray lines).

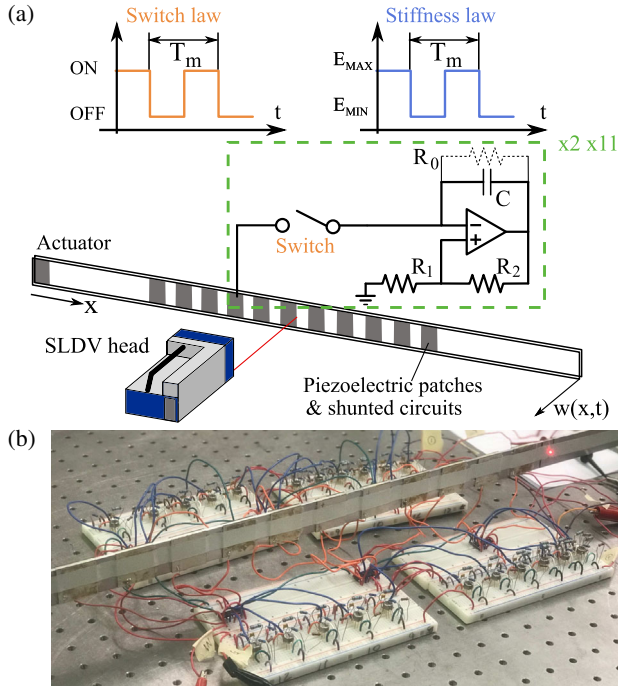


FIG. 4. Experimental setup for observation of the time-modulation of the stiffness in a beam through negative capacitance shunts and switches. (a) The beam is equipped with 11 pairs of piezoelectric patches, each connected to a NC circuit. (b) A switch opens and closes the patch-NC circuit series with a periodic law, inducing the stiffness to vary between two values with period T_m .

piezoelectric patches bonded to the beam and shunted through an electrical impedance (Fig. 4). The resulting electromechanical waveguide has an effective elastic modulus defined by the electrical impedance of the shunting circuit [38,39], which is the result of the strain-voltage coupling inherent to the piezoelectric effect. Resonant shunting circuits have been exploited to induce tunable band gaps in beam waveguides [40], while broadband stiffness control has been achieved through NC circuits

[41]. According to Refs. [41,42], the elastic modulus E_p^{SU} of a piezoelectric patch connected to a NC circuit with capacitance $-C'$ is given by:

$$E_p^{SU} = E_p^E \frac{C' - C_p^T}{C' - C_p^S}, \quad (7)$$

where E_p^E is the elastic modulus of the piezoelectric patch with short-circuited electrodes, C_p^T and $C_p^S = C_p^T(1 - k_{31}^2)$, respectively, are the stress-free and strain-free piezoelectric capacitance values, and k_{31} is the piezoelectric coupling coefficient for the longitudinal straining of a through-the-thickness polarized patch. Values of $C' > C_p^T$ ensure stability of the patch [33], while producing significant changes in the elastic modulus with respect to the open circuit value $E_p^D = E_p^E/(1 - k_{31}^2)$ for $|C'| \rightarrow 0$. The negative impedance converter circuit of Fig. 4(a) implements a capacitance $C_N = -C' = -R_2/R_1 C$ [41], where the resistor R_0 prevents saturation of the capacitor, which would lead to instability [42]. Operating a switch that breaks the series connection between the piezoelectric transducer and the NC shunt can vary the equivalent elastic modulus of the patch between the closed circuit (E_p^{SU}) and the open circuit (E_p^D) values [Eq. (7)]. Periodic on-off operation of the switch at period T_m induces a square-wave stiffness modulation at the fundamental frequency $\omega_m = 2\pi/T_m$. Based on beam configuration, and shunted piezoelectric parameters, the modulation amplitude obtained is $\alpha_m \approx 0.14$, which is estimated according to the procedure described in the Supplemental Material [43].

The experiments employ an array of 11 pairs of piezoelectric patches bonded to portion of a slender aluminum beam with rectangular cross section at regular spatial intervals (Fig. 4). All patches are connected in series to NC shunts (see Supplemental Material [43] for details on experimental setup). The beam is excited by a piezoelectric transducer bonded at its free end, which induces a transversely polarized wave propagating along the length. The

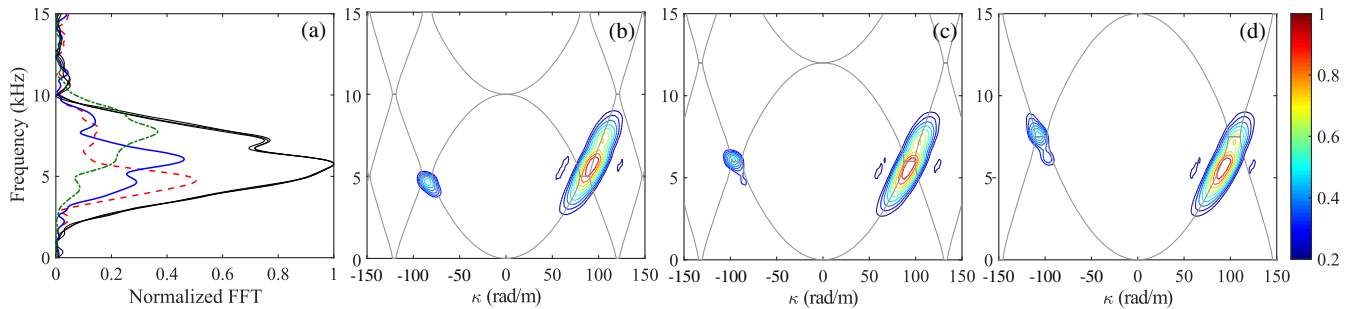


FIG. 5. Experimental results for the response of the beam waveguide for three modulation frequencies ($f_m = 10, 12, 15$ kHz). (a) Single point FTs show the conversion of a broadband input (black solid line) into narrow-band outputs centered at $f_m/2$: $f_m = 10$ kHz (red dashed line), $f_m = 12$ kHz (blue solid line), and $f_m = 15$ kHz (green dash-dotted line). (b)–(d) Normalized 2D-FT magnitude $|\hat{\mathcal{V}}(\kappa, \omega)|$ associated with the wave field $w(x, t)$ shows a narrow-band frequency reflection of the reflected waves in the $\kappa < 0$ half plane at $f_m/2$, which is in agreement with the location of the flat branches predicted theoretically (gray lines).

corresponding velocity field $w(x, t)$ is measured by a scanning laser Doppler vibrometer (SLDV). The recorded spatiotemporal wave field $w(x, t)$ is analyzed in the frequency–wave-number domain, where incident and reflected components are separated by identifying forward and backward propagating wave fields. This allows the separation of input $w^{(\text{in})}(x_p, t)$ and output $w^{(\text{o})}(x_p, t)$ components at the probe location x_p , which, as in the numerical investigations, is located near the interface.

Three experiments are performed by inducing a broadband excitation signal centered at 5 kHz, while modulating the effective stiffness at frequency $f_m = 10, 12, 15$ kHz. The analysis of the frequency spectrum of incident and reflected waves at the probe location [Fig. 5(a)] confirms that the reflected waves are characterized by a reduced bandwidth and centered at $f_m/2$. The half-power bandwidth of input and output signals is again evaluated in order to quantify the output-to-input bandwidth ratio. The input bandwidth is 3.2 kHz, while the output bandwidth is, respectively, 1.25, 1.14, and 1.61 kHz for $f_m = 10, 12, 15$ kHz. These correspond to 40%, 35%, and 50% output-input bandwidth ratios. Time modulation effects in terms of bandwidth and center frequency are also illustrated in the contour plots of Figs. 5(b)–5(d). While the dispersion branch associated with the incident wave in the $\kappa > 0$ region remains effectively unaltered in all three experiments, the reflected wave in the $\kappa < 0$ region is narrow band and centered at 5, 6, 7.5 kHz. We conclude that the system indeed behaves as predicted by it converting the broadband signal into a narrow-band signal at center frequency $f_m/2$.

In conclusion, we investigated time modulation effects in terms of reflected bandwidth and center frequency, and observed them experimentally for the first time through an electromechanical waveguide consisting of a beam in transverse motion, with an array of piezoelectric patches connected to switchable NC shunts. This enables control and periodic modulation of stiffness according to a square-wave law. Numerical and experimental results confirm the analytical predictions in terms of the existence of a wave number band gap characterized by flat real frequency bands and a nonzero imaginary frequency component. In the presence of an interface, this produces the selective reflection of an incident broadband wave at integer multiples of half the modulation frequency, which is a tuning parameter that determines the frequency content of reflected waves. The findings suggest an application of the concept as a single-port filtering device that can be tuned through the selection of the modulation frequency, and that may be implemented in acoustic, mechanical, or photonic platforms. The experimental implementation also provides a platform that allows the exploration of several unique properties associated with time and/or space modulation, including filtering, frequency conversion, nonreciprocity, PT symmetry, and topological pumping.

Support from the Air Force Office of Scientific Research Grant No. FA9550-15-1-0397 and from the Army Research Office Grant No. W911NF-18-1-0036 is acknowledged.

*yxia63@gatech.edu

- [1] J. C. Cullen, *Nature (London)* **181**, 332 (1958).
- [2] P. K. Tien, *J. Appl. Phys.* **29**, 1347 (1958).
- [3] G. Chao, *Appl. Phys. Lett.* **16**, 399 (1970).
- [4] F. W. Smith, *Electron. Lett.* **12**, 545 (1976).
- [5] J. C. Simon, *IEEE Trans. Microwave Theory Tech.* **8**, 18 (1960).
- [6] A. Hessel and A. A. Oliner, *IEEE Trans. Microwave Theory Tech.* **9**, 337 (1961).
- [7] E. S. Cassedy and A. A. Oliner, *Proc. IRE* **51**, 1342 (1963).
- [8] D. Holberg and K. Kunz, *IEEE Trans. Antennas Propag.* **14**, 183 (1966).
- [9] E. S. Cassedy, *Proc. IRE* **55**, 1154 (1967).
- [10] L. Felsen and G. Whitman, *IEEE Trans. Antennas Propag.* **18**, 242 (1970).
- [11] B. A. Auld, J. H. Collins, and H. R. Zapp, *Proc. IEEE* **56**, 258 (1968).
- [12] Y. Hadad, J. C. Soric, and A. Alu, *Proc. Natl. Acad. Sci. U.S.A.* **113**, 3471 (2016).
- [13] R. Fleury, D. L. Sounas, and A. Alù, *Phys. Rev. B* **91**, 174306 (2015).
- [14] Q. Wang, Y. Yang, X. Ni, Y. Xu, X. Sun, L. Chen, Z. Feng, X. Liu, M. Lu, and Y. Chen, *Sci. Rep.* **5**, 10880 (2015).
- [15] K. A. Lurie, *An Introduction to the Mathematical Theory of Dynamic Materials*, Advances in Mechanics and Mathematics (Springer, New York, 2007).
- [16] D. L. Sounas and A. Alù, *Nat. Photonics* **11**, 774 (2017).
- [17] K. Yi, M. Collet, and S. Karkar, *Phys. Rev. B* **96**, 104110 (2017).
- [18] G. Trainiti and M. Ruzzene, *New J. Phys.* **18**, 083047 (2016).
- [19] K. Fang, Z. Yu, and S. Fan, *Phys. Rev. Lett.* **108**, 153901 (2012).
- [20] D.-W. Wang, H.-T. Zhou, M.-J. Guo, J.-X. Zhang, J. Evers, and S.-Y. Zhu, *Phys. Rev. Lett.* **110**, 093901 (2013).
- [21] T. T. Koutserimpas and R. Fleury, *Phys. Rev. Lett.* **120**, 087401 (2018).
- [22] D. Torrent, O. Poncelet, and J.-C. Batsale, *Phys. Rev. Lett.* **120**, 125501 (2018).
- [23] J. Vila, R. K. Pal, M. Ruzzene, and G. Trainiti, *J. Sound Vib.* **406**, 363 (2017).
- [24] N. Swintek, S. Matsuo, K. Runge, J. O. Vasseur, P. Lucas, and P. A. Deymier, *J. Appl. Phys.* **118**, 063103 (2015).
- [25] R. Fleury, A. B. Khanikaev, and A. Alù, *Nat. Commun.* **7**, 11744 (2016).
- [26] H. Nassar, X. Xu, A. Norris, and G. Huang, *J. Mech. Phys. Solids* **101**, 10 (2017).
- [27] J. Gump, I. Finkler, H. Xia, R. Sooryakumar, W. J. Bresser, and P. Boolchand, *Phys. Rev. Lett.* **92**, 245501 (2004).
- [28] A. Bellino, A. Fasana, E. Gandino, L. Garibaldi, and S. Marchesiello, *Mech. Syst. Signal Process.* **47**, 120 (2014).

- [29] C. Croënne, J. O. Vasseur, O. B. Matar, M.-F. Ponge, P. A. Deymier, A.-C. Hladky-Hennion, and B. Dubus, *Appl. Phys. Lett.* **110**, 061901 (2017).
- [30] M.H. Ansari, M.A. Attarzadeh, M. Nouh, and M.A. Karami, *Smart Mater. Struct.* **27**, 015030 (2018).
- [31] A. Nanda and M. A. Karami, *ASME Conf. Smart Mater., Adapt. Struct. Intell. Syst.* **2**, V002T03A030 (2017).
- [32] Y. Wang, B. Yousefzadeh, H. Chen, H. Nassar, G. Huang, and C. Daraio, *Phys. Rev. Lett.* **121**, 194301 (2018).
- [33] B. de Marneffe and A. Preumont, *Smart Mater. Struct.* **17**, 035015 (2008).
- [34] G. W. Milton and O. Mattei, *Proc. R. Soc. A* **473**, 20160819 (2017).
- [35] S. V. Suchkov, A. A. Sukhorukov, J. Huang, S. V. Dmitriev, C. Lee, and Y. S. Kivshar, *Laser Photonics Rev.* **10**, 177 (2016).
- [36] J.R. Zurita-Sánchez, P. Halevi, and J.C. Cervantes-González, *Phys. Rev. A* **79**, 053821 (2009).
- [37] M. Ruzzene, *Smart Mater. Struct.* **16**, 2116 (2007).
- [38] R. L. Forward, *Appl. Opt.* **18**, 690 (1979).
- [39] N. Hagood and A. von Flotow, *J. Sound Vib.* **146**, 243 (1991).
- [40] L. Airoldi and M. Ruzzene, *New J. Phys.* **13**, 113010 (2011).
- [41] S. Behrens, A. J. Fleming, and S. O. R. Moheimani, *Smart Mater. Struct.* **12**, 18 (2003).
- [42] B. S. Beck, K. A. Cunefare, and M. Collet, *Smart Mater. Struct.* **22**, 065009 (2013).
- [43] See Supplemental Material at <http://link.aps.org/supplemental/10.1103/PhysRevLett.122.124301> for equivalent stiffness change estimation, data acquisition and experimental parameters.